Research article

Pb(II)-phycoremediation mechanism using *Scenedesmus obliquus*: cells physicochemical properties and metabolomic profiling

M. Danouche [a,b,*], N. El Ghachtouli [b,**], A. Aasfar [a], I. Bennis [a], H. El Arroussi [a,c]

[a] *Green Biotechnology Center, Moroccan Foundation for Advanced Science, Innovation and Research (MAScIR), Rabat, Morocco*
[b] *Microbial Biotechnology and Bioactive Molecules Laboratory, Sciences and Technologies Faculty, Sidi Mohamed Ben Abdellah University, Fez, Morocco*
[c] *AgroBioScience (AgBS), Mohammed VI Polytechnic University (UM6P), Ben Guerir, Morocco*

ARTICLE INFO

ABSTRACT

This study highlights the mechanisms of Pb(II)-phycoremediation using the Pb(II) tolerant strain of *Scenedesmus obliquus*. First, monitoring of cell growth kinetics in control and Pb(II)-doped medium revealed significant growth inhibition, while the analyses through flow cytometry and Zetasizer revealed no difference in cell viability and size. Residual weights of control and Pb(II)-loaded cells assessed by thermogravimetric analysis were 31.34% and 57.8%, respectively, indicating the uptake of Pb(II) into *S. obliquus* cells. Next, the use of chemical extraction to distinguish between the intracellular and extracellular uptake indicated the involvement of both biosorption (85.5%) and bioaccumulation (14.5%) mechanisms. Biosorption interaction of Pb(II) ions and the cell wall was confirmed using SEM-EDX, FTIR, zeta potential, zero-charge pH, and contact angle analyses. Besides, the biochemical characterization of control and Pb(II)-loaded cells revealed that the bioaccumulation of Pb(II) induces significant increases in the carotenoids and lipids content, while it decreases in the chlorophyll, carbohydrates, and proteins content. Finally, the metabolomic analysis indicated an increase in the relative abundance of fatty acid methyl esters, alkanes, aromatic compounds, and sterols. However, the alkenes and monounsaturated fatty acids decreased. Such metabolic adjustment may represent an adaptive strategy that prevents high Pb(II)-bioaccumulation in cellular compartments.

1. Introduction

Since the Earth's formation, nearly all the heavy metals (HMs) that we know today have been present naturally in trace amounts and have been recycled biogeochemically between the environmental compartments, through biotic and abiotic biogeochemical processes (Garrett, 2000). However, anthropogenic activities, such as mining, excessive use of fertilizers in agriculture, and mismanagement of hazardous wastes have increased the redistribution of HMs among the environmental compartments, leading to increased HMs-pollution in the aquatic and terrestrial ecosystem (Ashraf et al., 2014). Indeed, because they are not biodegradables, HMs can persist in these ecosystems and can bioaccumulate into organisms of different trophic levels, causing therefore various signs of toxicity to all life forms (Yan et al., 2018). Mercury (Hg(II)), cadmium (Cd(II)), lead (Pb(II)), arsenic (As(III)), and chromium (Cr(VI)) are among the most harmful pollutants (Kumar et al., 2015). According to the regulations of the U.S. Environmental Protection Agency (EPA), the

maximum contamination limits of these HMs are 0.002, 0.005, 0.015, 0.01, and 0.1 mg L^{-1}, respectively (USEPA, 2016). Unfortunately, their actual concentrations in industrial wastewater are higher than these standards. It is therefore necessary to carry out an adequate treatment before their discharge into the environment (Selvi et al., 2019). For example, the presence of Pb(II) ions in aquatic ecosystems, even at low concentrations causes a wide range of toxic effects on the physiological, biochemical, and metabolic functions of the exposed organisms (microorganisms, plants, and animals), and human health risks caused by direct exposure to HMs or through consumption of contaminated food or water (Lee et al., 2019).

Recently, the pollution of water by HMs has piqued the interest of scientists, conservationists, and politicians. Indeed, various techniques, including precipitation, adsorption, nano/ultrafiltration, reverse osmosis, electrochemical technologies, and biological approaches have been applied to remove HMs from contaminated water bodies (Kumar et al., 2015). Because bioremediation approaches are effective,

---

* Corresponding author.
** Corresponding author.
E-mail addresses: mohammed.danouche@usmba.ac.ma (M. Danouche), naima.elghachtouli@usmba.ac (N. El Ghachtouli).

environmentally friendly, and inexpensive, they appear to be competitive to the conventional physicochemical procedures (Chibueze et al., 2016; Danouche et al., 2021c). The application of microalgae in wastewater treatment has recently emerged as a promising solution because of its advantages over the other conventional methods (Wollmann et al., 2019). To differentiate the use of microalgae from the other biological approaches, this (bio)procedure is called phycoremediation (Jais et al., 2017). It has been documented that phycoremediation has been applied for the removal of Pb(II) ions from contaminated waters. Some of these studies only highlight the potential application of inactive biomass of microalgae species as biosorbents (Kumar et al., 2008). While only a few researchers have described the potential application of living microalgae for the Pb(II)-bioremoval (Liyanage et al., 2020; Pham et al., 2020; Piotrowska-Niczyporuk et al., 2015), even though the use of growing cells is more advantageous because it avoids the steps of cultivation, harvesting, drying, and conservation of biomass before their use as biosorbents (Danouche et al., 2021a). In addition, the use of growing microalgae will improve removal efficiency through both metabolism-independent (biosorption) and metabolism-dependent (bioaccumulation) mechanisms (Kumar et al., 2015).

On the other hand, under metal-stressed conditions, living cells of microalgae can produce various high-value substances such as polymeric substances, proteins, pigments, and lipids (Liu et al., 2016). Thus, they offer a real possibility of exploitation in various industrial sectors, mainly in the field of renewable energies (Ansari et al., 2019; Liu et al., 2016). Consequently, understanding the influence of HMs on the biochemical composition of green microalgae is critical for a targeted valorization of the biomass and/or the metabolites produced during the phycoremediation process. Several studies have investigated the economic aspects of combining wastewater treatment and the valorization of the biomass in various value-added products, especially lipids, as a source of third-generation biofuels (Ansari et al., 2019; Randrianarison and Ashraf, 2017).

The use of omics approaches such as metabolomics can help to advance the insight of the phycoremediation mechanisms (Danouche et al., 2021b), as well as for the valorization of high-value-added metabolites produced under metallic stress (Jamers et al., 2009; Salama et al., 2019). In terms of metabolomic tools, liquid chromatography-mass spectrometry (LC-MS), gas chromatography-mass spectrometry (GC-MS), and proton nuclear magnetic resonance (^{1}H-NMR) are the main analytical platforms adopted in metabolomic studies. However, ^{1}H-NMR suffers from low sensitivity and may not detect low-abundance metabolites compared to other techniques (Ong et al., 2009). Over the past few years, the combination of gas chromatography-quadrupole time-of-flight mass spectrometry (GC-Q-TOF/MS) and liquid chromatography-quadrupole time-of-flight mass spectrometry (LC-Q-TOF/MS) has been successfully applied in many metabolomic studies in order to achieve more sensitive and accurate metabolic profiling (Wang et al., 2018).

The present study aims to investigate the phycoremediation mechanism of Pb(II) ions using living cells of Pb(II)-tolerant strain of *Scenedesmus obliquus*. Firstly, the physicochemical properties of the cells before and after Pb(II) phycoremediation were evaluated to investigate the extracellular elimination mechanisms between the cell surface and Pb(II) ions in solution. Thereafter, the changes in biochemical composition and the metabolomic profiling of cells were examined after Pb(II) bioaccumulation to identify the resistance strategies of this strain toward Pb(II) ions.

2. Material and methods

2.1. Microalgae strain and culture condition

The green microalgae *Scenedesmus obliquus* used in this study has been previously selected as a high Pb(II)-tolerant strain, with a half-maximal effective concentration (EC$_{50}$) of 141 ppm, and removal efficiency of 58.42% from this initial concentration (Danouche et al., 2020).

Its unialgal culture was sub-cultured at regular times in BG$_{11}$ medium (1.5 g NaNO$_3$, 40 mg K$_2$HPO$_4$, 36 mg CaCl$_2$ 2H$_2$O, 6 mg ammonium citrate monohydrate, 6 mg ammonium ferric citrate, 1 mg ethylenediaminetetraacetic acid (EDTA), 2.86 mg H$_3$BO$_3$, 1.81 mg MnCl$_2$ 4H$_2$O, 0.22 mg ZnSO$_4$ 7H$_2$O, 0.39 mg NaMoO$_4$ 5H$_2$O, 0.079 mg CuSO$_4$ 5H$_2$O, 0.050 mg CoCl$_2$ 6H$_2$O in 1 L of distilled water) (Allen, 1968). The experiments were performed with a unialgal culture of *S. obliquus* obtained at the exponential phase. Biomass was firstly recovered by centrifugation at 4700 rpm for 10 min. Then, the pellet was diluted in Erlenmeyer flasks containing 100 mL of BG$_{11}$ medium for negative control and Pb(II)-doped medium at the concentration of EC$_{50}$ = 141 mg L^{-1} (Danouche et al., 2020). The initial optical density (OD) of all experiments was adjusted to 0.350 ± 0.025 at A$_{680nm}$ using Ultrospec™ 3100 pro UV-Visible spectrophotometer, corresponding to 2 x 10^6 cells mL^{-1} equivalent. Flasks were incubated under controlled conditions at 25 ± 2 °C, under rotary shaking conditions at 150 rpm, and 10 h:14 h light-dark cycle.

2.2. Pb(II)-phycoremediation mechanism

Pb(II)-uptake biosorption and/or bioaccumulation was firstly evaluated using thermogravimetric analysis (TGA). The changes in weight of samples while heated to a constant temperature under an inert atmosphere were measured using TGA Q500 - Emballage - TA Instruments - USA. An equal weight of the biomass samples was first placed in a platinum pan, then heated up to 600 °C under a nitrogen-controlled atmosphere, at a heating rate of 10 °C min^{-1} (Sudhakar and Premalatha, 2015). Finally, the TGA, as well as the difference thermogravimetry ratio (DTG) of the control and Pb(II)-loaded cells was plotted using excel software.

The discrimination between the intracellular biosorption and the extracellular bioaccumulation of Pb(II) was carried out using chemical extractions as reported by Hassler et al. (2004): after the phycoremediation process, the biomass was recovered by centrifugation (4700 rpm for 10 min), the pellet samples were washed with EDTA solution (5.10^{-3} M; pH 6.0). Next, dried biomass (washed and unwashed) were digested with 65% HNO$_3$ and 30% H$_2$O$_2$ in ACCblock digital dry bath (Labnet) for 40 min at 140 °C. Pb(II) concentration in the mineralized samples was measured using a Thermofisher 7000 series inductively coupled plasma optical emission spectrometer (ICP-AES). Thus, the bioadsorbed Pb(II) onto the cells' surface was determined by subtracting the intracellular Pb(II) concentration from the total Pb(II) removed (Huang et al., 2004).

2.2.1. Physicochemical characterization of Pb(II)-biosorption
Scanning electron microscope coupled with Energy-dispersive X-ray spectroscopy (SEM-EDX): SEM (JSM-IT500 InTouchScope™) was used to visualize the cells' surface of *S. obliquus* before and after Pb(II)-biosorption. While, the EDX was employed to analyze the elemental composition from the imaged area. The analysis conditions were a SED signal, under x1,000 - x55,000 magnification, and 3.0 kV landing voltage, with a working distance of 10.1 mm, at high vacuum mode.

Fourier Transform InfraRed spectroscopy (FTIR) analysis: to predict the functional groups on the cell wall, the biomass from the control and Pb(II)-doped medium were analyzed using FTIR spectroscopy. Salt pellets were firstly prepared using 1 mg of dried biomass and 149 mg of KBr, then compressed at 40 kN for 5 min to form pellets. Finally, thirty-two scans were performed at a range of 400–4000 cm^{-1}, with 4 cm^{-1} of resolution for each sample, using the ABB Bomem FTLA 2000 spectrometer analyzer (Das et al., 2016).

Zeta potential and Zero-point charge measurement: In order to determine the zeta (ζ) potentials of the biosorbents as a function of pH, a 100 mL volume of microalgae suspension was harvested by centrifugation (4700 rpm for 10 min), then the pellet was resuspended in 10 mL of NaCl (0.1 M). The pH of the suspensions was adjusted from 3 to 10 with 0.1 M of HCl or NaOH solutions. The ζ-potential was evaluated in the

electrophoresis cell at 25 °C using Nanosizer Nano (Malvern). For each pH value, triplicate measurements were taken, and approximately 30 readings were done for each data (Hadjoudja et al., 2010).

The electrical state of the microalgae surface in solution was characterized using a zero-charge point (pHzc). Briefly, NaCl solutions (0.1 M) with pH ranging from 3 to 10 were prepared. Aliquots of 10 mL of each pH-adjusted solution were mixed with 50 mg of the biomass, shaken for 24 h at 25 °C, then the final pH values were measured. The difference in ΔpH was plotted against the initial pH_i to determine the pHzc (Zehra et al., 2016).

Contact angle measurements: measurement of the contact angle of *S. obliquus* cells from the control and Pb(II)-doped medium was carried out at 25 °C as described by Asri et al. (2018) using a digital optical contact angle (Data Physics OCA 40), via the sessile drop method, using water, formamide, and diiodomethane (Table 1). Both the left and the right contact angle measurements of both biomasses were automatically calculated from the digitalized image using SCA 20 software for OCA and PCA operated under Windows 7. The hydrophobicity degree of the control and Pb(II)-loaded cells were estimated according to Vogler's and Van Oss approach (Van Oss et al., 1988; Vogler, 1998).

2.2.2. Physiological and biochemical response to Pb(II)-bioaccumulation

Growth monitoring: growth kinetics of *S. obliquus* in control and Pb(II)-doped medium were monitored spectrophotometrically at two-day intervals. The linear relationship between microalgal density (N, in cells per milliliter) and OD_{680nm} was determined as reported by Zhou et al. (2012) using a CKX41 Olympus light microscope and a Malassez counting chamber, with a depth of 0.2 mm. The calibration curve was as Eq. (1):

$$Y = 7. 10^6 X + 2083 \ (R^2 = 0.98) \tag{1}$$

where Y is the number of cells (C mL^{-1}) and X denotes the OD at 680_{nm}.

Membrane integrity: As described by da Silva et al. (2009), the membrane integrity of *S. obliquus* cells grown in control and Pb(II)-doped medium was performed. An amount of 10^6 cells were centrifuged at 4700 rpm for 10 min. Pellet was then washed with phosphate buffer solution (PBS, pH 7.0). Next, the cells were then exposed to 10 μg mL^{-1} of propidium iodide (PI, Ref 81845 FLUKA). The reaction was maintained in the dark for 10 min and directly analyzed by BD FACSCalibur Flow Cytometry (FCM) System (BD Biosciences). PI is a fluorescent intercalating agent that intersperses with the double-stranded nucleic acids to produce red fluorescence when excited by blue light. Undamaged membranes of living microalga are impermeable to PI. While, due to the loss in the membrane integrity, the dye can be input to the intracellular compartment of stressed cells (Suman et al., 2015). Heat-inactivated cells were primed for positive control and processed under the same conditions. The fluorescent emission of PI was collected from ~3000 events per sample. The PI was excited at 488_{nm} and measured at 585_{nm} (FL_2 channel) using the FACSCalibur optical system. Parameter settings were adjusted to place the non-stained population in the negative area FL_2/FL_1 as an autofluorescence control. Data were processed with CELLQuest Pro software (Becton Dickinson) and expressed as fluorescence arbitrary units. The viability of cells was expressed as the percentage of cells viable versus the total number of cells acquired (Asghari et al., 2019; Urrutia et al., 2019).

Cells size: Pb(II) effect on the osmotic state of *S. obliquus* cultured in control and Pb(II)-doped medium was carried out based on the change in cell size, using the Malvern Zetasizer Zeta-Nano (England), working with laser doppler electrophoresis technique. The dynamic light scattering (DLS) method was used to determine the changes in cells size after Pb(II)-phycoremediation (Xia et al., 2017).

Ion flows and osmoregulators' accumulation: For further insight into the Pb(II)-bioremoval mechanism using *S. obliquus*. The intracellular concentrations of both Na^+, K^+ ions were also analyzed. The decomposition of samples and the measurement of Na^+, K^+ concentrations were performed as described for Pb(II) determination using ICP-AES. Proline (Pro) accumulation as a marker of osmoregulation was performed as described by Cervantes-García et al. (2011), samples of both biomasses were homogenized in 3 mL of sulfosalicylic acid (3%), centrifuged at 4000xg for 15 min, then the supernatants were added with a solution of 2.5% acidic ninhydrin and glacial acetic acid and incubated for 45 min in a boiling water bath. Finally, an equal volume of toluene was added and the absorbance was read at $A520_{nm}$ (Bates et al., 1973).

Photosynthetic pigments analysis: Pb(II)-impact on the photosynthetic system was firstly evaluated based on the cellular autofluorescence using the FCM system. When cells are excited by red (635_{nm}) and blue (488_{nm}) diode lasers, the chlorophyll can be observed in both orange (FL_2: 585/42 nm) and red (FL_3: 530/30 nm) channel. Phycoerythrin (PE) is excited with the argon laser (488_{nm}) and emits in the orange region, their fluorescence can be measured at the FL_2. When phycocyanin is excited by a diode laser, it emits fluorescence in the (661/16 nm) channel.

The pigments content was also assayed spectrophotometrically using the method of Tahira et al. (2019). Preparation of pigment extract from control cells and Pb(II) accumulated cells was performed at a concentration of 1 mg mL^{-1} in 95% ethanol. Next, samples were homogenized using a SONOPULSmini20 ultrasonic homogenizer at 4 °C and kept overnight in the dark at 4 °C. after centrifugation (10 min at 4700 rpm), the absorbance was measured at 470_{nm}, 649_{nm}, and 664_{nm}, and the contents of chlorophyll a (Ch-a), chlorophyll b (Ch-b), and the total carotenoids (C x_+c) were calculated based on Lichtenthaler and Buschmann (2001) Eqs. (2), (3), and (4).

$$Ch\text{-}a = 13.36 \ A_{664} - 5.19 \ A_{649} \tag{2}$$

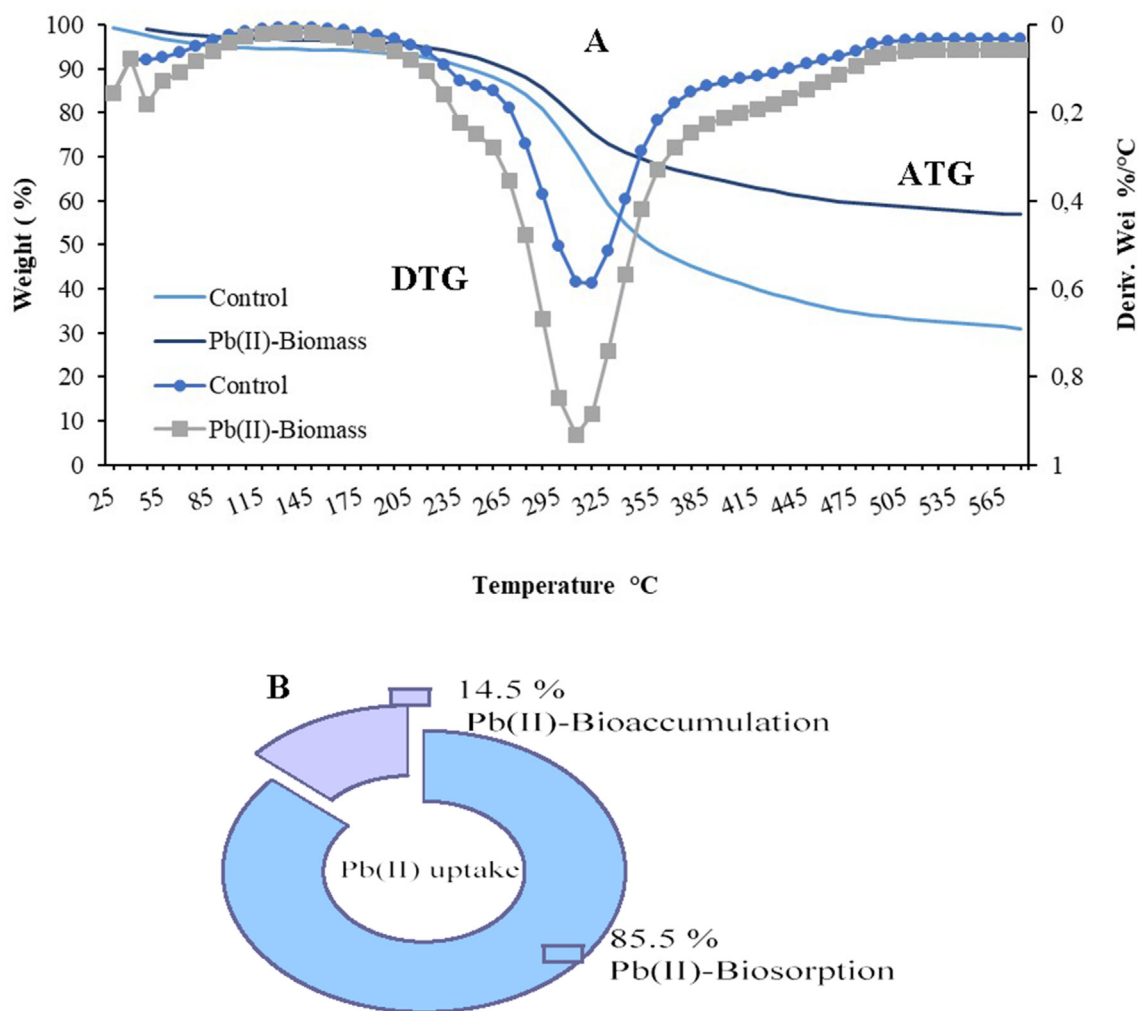$$Ch\text{-}b = 27.43 \ A_{649} - 8.12 \ A_{664} \tag{3}$$

$$C \ x_+c = (1000 \ A_{470} - 2.13 \ Ch\text{-}a - 97.63 \ Ch\text{-}b)/209 \tag{4}$$

Proteins, lipids, and carbohydrates determination: Extraction of lipids and their quantification were achieved as reported by El Arroussi et al. (2017) using a solvent mixture of water: chloroform: methanol (1:2:1). After homogenization, the biomass mixture was centrifuged (5 min at 4700 rpm), and the chloroform layer was recovered and evaporated using nitrogen gas, finally the total lipids were weighed.

The estimation of neutral lipid content in cells of *S. obliquus* from control and Pb(II)-doped medium was also evaluated employing the multi-parameter FCM with the fluorescent stain Nile Red (NR) as reported by da Silva et al. (2009). Lipids' straining with NR is traduced to different fluorescence emissions after excitation with the argon laser at 488_{nm}. When NR is dissolved in neutral lipids, it emits an intense yellow fluorescence collected in the FL_2 channel. When dissolved in polar lipids, it exhibits red fluorescence collected in the FL_3 channel (Jara et al., 2003).

Regarding the extraction of proteins, 50 mg of lyophilized biomass was homogenized using the ultrasonic homogenizer in an ice bath assisted by freezing cycles thawing at -80 °C. The homogenate was next centrifuged at 4700 rpm for 15 min at 4 °C. Then, the supernatant was used for the estimation of the total soluble proteins via the Bradford method, and bovine serum albumin as standard (Bradford, 1976).

Total soluble sugars were estimated using the protocol described by Wychen and Laurens (2017), the biomass was first hydrolyzed by

Table 1. Energy characteristics [Lifshitz-van der Waals (Υ^{LW}), electron-donor (Υ^-), and electron-acceptor (Υ^+) parameters (mJ.m^{-2})] of the liquids used.

Liquids	Surface energy parameters (mJ m^{-2})		
	Υ^{LW}	Υ^+	Υ^-
Water (θ_w)	21.8	25.5	25.5
Formamide (θ_F)	38.7	2.3	39.4
Diiodomethane (θ_D)	50.5	0.7	0

Figure 1. (A) plots the TGA and DTG profile of the decomposition of controlled and Pb(II)-loaded cells. (B) illustrates the rate of bioaccumulation and biosorption of Pb (II) ions by living cells of *S. obliquus*.

two-step sulfuric acid hydrolysis first in 72% (w/w) sulfuric acid for 1 h at 30 °C. Then, placed in an autoclave for 1 h at 121 °C with 4% (w/w) sulfuric acid. Finally, the total soluble carbohydrate content was assessed via the phenol-sulfuric acid colorimetric method (Dubois et al., 1956).

2.2.3. Metabolomics response to Pb(II) bioaccumulation

Metabolomics profiling of *S. obliquus* cultivated in control and Pb(II)-doped medium were analyzed using a Gas Chromatography-Mass Spectrometry (GC-MS) (Agilent 7890A Series GC). Both biomasses were recovered by centrifugation (4700 rpm for 10 min), then transferred to 15 mL conical centrifuge tubes prepared in a dewar filled with liquid nitrogen. For the extraction of non-polar metabolites, a solvent mixture of water, chloroform and methanol (1:2:1) was employed (El Arroussi et al., 2017).

Non-polar metabolites determination: the transesterification reaction was performed using 6% H_2SO_4-methanol at 80 °C, and atmospheric pressure during 3 h, assisted by ultrasonication in Branson ultrasonic (Soniffier 450) bath at 40 kHz (Chanda et al., 2020). 2 mL aliquots of chloroform-solubilized metabolites were analyzed by GC, using split mode (1:4) with the helium at 1.5 mL min^{-1} as carrier gas. The ion source and quadruple temperatures were 230 °C and 150 °C respectively. The oven temperature program started at 30 °C, it was then increased by 10 °C min^{-1} to 120 °C, increased until 200 °C by 30 °C min^{-1}, increased to

250 °C by 10 °C min^{-1}, temperature and hold for 1 min at the end of each phase. Finally, the temperature was increased to 270 °C by 5 °C min^{-1} and kept constant for 5 min. The detection was achieved by full scan mode between 30 and 1000 m/z, with a gain factor of 5 (El Arroussi et al., 2015).

Metabolite identification and data normalization: metabolites detected by GC-MS were identified with MS NIST 2014 library, as having predictability greater than 90%. Their classification was carried out by PubChem and LIPID MAPS database. To correct the heteroscedasticity and the pseudo-scaling, the power transformation was applied (van den Berg et al., 2006). The amounts of each metabolite were calculated based on the peak areas using dodecane as standard.

2.3. Statistical analysis

The experiments were carried out in triplicate, and data were expressed as the mean ± standard deviation. Statistical significance of biochemical analysis results between cells of *S. obliquus* from the control and Pb(II)-doped medium was performed with unpaired T-test, and two-way ANOVA by Sidak's multiple comparisons test using GraphPad Prism software version 8.0. P-values below 0.05 were considered statistically significant. The generation of heat map was performed using RStudio, and the visualization by FactoMineR package.

3. Results and discussion

3.1. Pb(II)-phycoremediation mechanisms

For a detailed understanding of the mechanisms involved in Pb(II) phycoremediation by *S. obliquus*, TGA and DTG profiles of control and Pb(II)-loaded biomass were firstly analyzed. The results presented in Figure 1A indicate that there are three phases of the biomass decomposition. The first stage, from 25 to 250 °C corresponds to the weight loss process of volatile compounds, the second stage (from 250 to 445 °C) belongs to the devolatilization process, and the third stage (over 445 °C)

consistent with the slow decomposition of the inorganic residue of ash, resulting from the previous step. Also, the rate of residue weight of cells after Pb(II)-biosorption (57.8%) was higher than that of cells from the control medium (31.34%). These results agree with previous research. For instance, Marcilla et al. (2009) noted that the TGA and the DTG of the thermal pyrolysis of *Nannochloropsis* sp. have also three main decomposition steps (<180 °C, 180–540 °C, and >540 °C). It is clearly illustrated in Figure 1A that the rate of residue weight of cells after Pb(II)-biosorption (57.8%) was higher than that of control cells (31.34%). Moreover, the DTG showed that the weight loss at 315 °C was 0.588% for control biomass, and 0.346% for Pb(II)-loaded cells. The
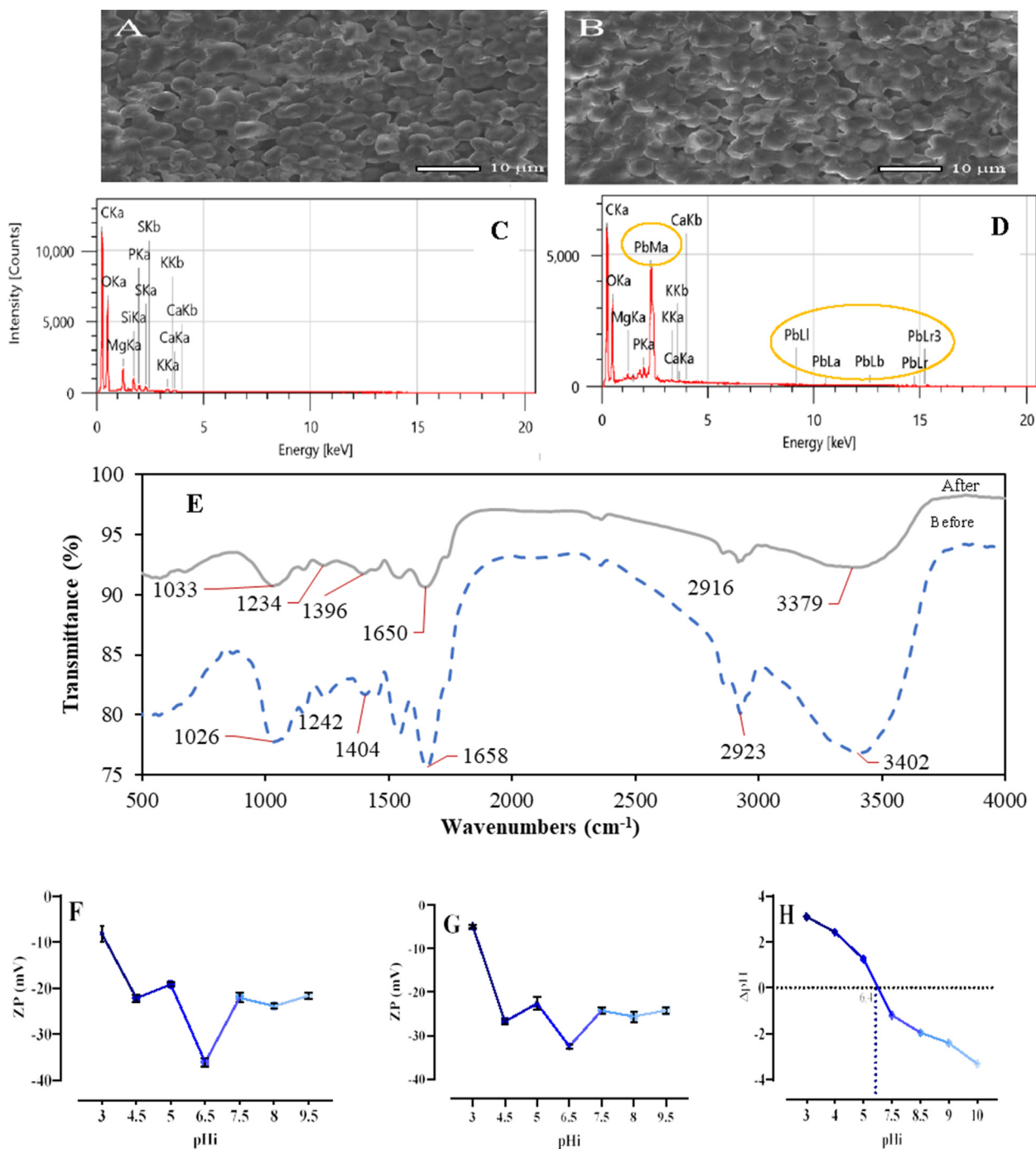
Figure 2. Displays SEM image of (A) control cells; (B) Pb(II)-loaded cells at x8000 magnification. The selected X-ray spectra of control (C), Pb(II)-loaded cells (D), FTIR spectra of control and Pb(II)-loaded cells (E), ζ-potential of control (F) and Pb(II)-loaded cells (G). Zero-charge pH loading (H) of *S. obliquus* biomass in the pHi range of 3–10.

difference in weight loss would be related to the composition of the cells after Pb(II)-uptake. In this way, Venkata Mohan et al. (2007) stated that the heat required for thermal degradation of *Spirogyra* sp. was higher after biosorption of fluoride, compared to the control cells, which could be the result of the ionic bond formed after biosorption.

Subsequently, the discrimination between extracellular biosorption and intracellular bioaccumulation was examined. As presented in the pie chart of Figure 1B, the concentration of Pb(II) in washed and unwashed cells was 9.2 mg L^{-1} and 54.2 mg L^{-1}, respectively. This suggests that both mechanisms: bioaccumulation (14.5%) and biosorption (85.5%) are implicated in the Pb(II)-phycoremediation process. Among the few types of research that have been focused on the discrimination between the intracellular bioaccumulation and the extra-cellular biosorption mechanisms. Elleuch et al. (2021) showed that the efficiency of Pb(II) removal depended on microalgal strains (*Amphora coffaeiformis, Navicula salinicola,* and *Dunaliella salina*) by means of both intracellular bioaccumulation and surface biosorption mechanisms. Also, Pérez-Rama et al. (2002) reported that the bioremoval of Cd(II) by living cells of *Tetraselmis suecica* involves both mechanisms, intracellular bioaccumulation, and extra-cellular biosorption. For the remainder of this study, an in-depth analysis of these two mechanisms was therefore performed.

3.1.1. Physicochemical characterization of Pb(II)-biosorption

Given that biosorption is the main mechanism involved in the removal of Pb(II) ions by *S. obliquus*. We first performed SEM and EDX analyses to investigate the variations in the cell surface, as well as their elemental composition. Figure 2A and B display respectively the SEM images of control cells and after Pb(II)-biosorption at 8000× magnification. Notable differences in cells appearance were observed in Pb(II)-loaded cells compared to the control. Indeed, a white appearance appears on the cells after Pb(II) biosorption, which reflects the absorption of Pb(II) ions on the cell surface. The X-ray analysis confirmed these observations. As shown in Figure 2C, the peaks representing C, P, O, S, K, Mg, Ca, and Si in control cells may be attributed to the biological components of the cell wall. Whereas, a notable change was observed in the elemental composition of Pb(II)-loaded cells, with a disappearance of the peaks corresponding to Si and S in the region 2.2–2.3 KeV. These peaks were substituted by a Pb corresponding peak after the phycoremediation process. Moreover, there was a variation in the intensity level of the other elements detected. Based on those results, there were two peaks region related to the presence of Pb(II) in cells of *S. obliquus*, the first was on the low-energy region (2.2 KeV), and five other peaks related to Pb(II) were detected on the high-energy region of the spectrum (Figure 2D), confirming the variation in the distribution of Pb(II) accumulation onto *S. obliquus*. Indeed, Pb(II) ions can pass from the cell wall to the biological membrane and be bioaccumulated in the intracellular compartment (Blaby-Haas and merchant, 2012), whereas a large amount of Pb(II) was biosorbed on the cell surface. This finding conforms to the results of ICP and TGA analyses.

Figure 2E depicts the FTIR spectra of *S. obliquus* before and after Pb(II)-phycoremediation, showing a heterogeneous composition of the cell wall, characterized by the presence of several peaks' characteristic of lipids, proteins and carbohydrates. Indeed, a significant changes in these functional groups were noted after Pb(II) biosorption. The absorption peaks at the region between 3200 and 3600 cm^{-1} indicated the existence of stretching vibration of hydroxyl (-OH) and amino (-NH$_2$) groups, which are among the functional groupings of chitosan and amino acids. The peaks around the region 3000 - 2800 cm^{-1} showed the stretching vibration functional of Methyl, and Methylene groups (-CH$_3$, –CH$_2$-). The peaks at 1650 and 1542 cm^{-1} would be caused by the bending and stretching of amine (-R$_2$-NH) groups of the proteins. The peaks around 1400 and 1200 cm^{-1} may be caused by phosphorous groups (-PO-) that compose the phospholipid membrane. The peaks at 1026 cm^{-1} elongation of bonds (C–C), (C–O), and (C–N) correspond to the polysaccharides (He and Chen, 2014). These functional groups have been previously identified on the cell wall of various microalgae species (Zheng et al., 2016). After Pb(II)-biosorption, a significant decrease in the transmittance of these peaks was recorded, which may be attributed to its occupation by Pb(II) ions. Furthermore, the comparison of FTIR spectra of biomass before and after Pb(II) biosorption showed a shift in some functional groups, mainly in the absorption bands of hydroxyl, carboxylic acid, amine and amino groups. This finding, suggests that the biosorption of Pb(II) involves several interactions between the cells' surface and the ions from the solution (Tran et al., 2017). Some previous studies indicated also that the biosorption process was accomplished by chelation and formation of ionic bridges between HMs and the functional groups (Gupta and Rastogi, 2008; Jena et al., 2015).

The measurement of ζ-potential, as well as the pHzc are among the key parameters related to the external loads of the adsorbent (Akar et al., 2009). As shown in Figure 2F, the ζ-potential of *S. obliquus* was maintained at a negative charge, regardless of the initial pH value. Indeed, it varied from -8.17 mV at pH 3 to -36.13 at pH 6.5. This result testifies the anionic characteristics and the high concentration of acid groups on the cell wall. At the pHi value, the ζ-potentials of cells from the control medium (-36.13 mV) was higher than those of Pb(II)-loaded microalgal cells (-32.5 mV) (Figure 3F and G). The value of pHz at which the ΔpH = 0 was at 6.45 (Figure 3H), confirming the dominance of anion groups over cation groups on the cell's surface. These negatively charged groups facilitate the binding of ions to the cell surface, making the outer layer of the cell wall the primary participant in the removal of HMs (Leong and Chang, 2020; Saavedra et al., 2018; Singh et al., 2021). These findings are consistent with previous research. Li et al. (2017) showed that the ζ-potential of *Desmodesmus bijugatus, Botryococcus* sp, and *Chlorella* sp was negatively charged during all growth phases. Also, Samadani et al. (2018) reported that the average of the ζ-potential of *Chlamydomonas* was at - 41 mV, - 4mV for both pH 7 and pH 4, respectively. At low pH, the ζ-potential around to zero can reduce the electrostatic interactions of HMs and the cell surface, reducing thereby the cationic fluxes into the cells.

Based on both Vogler's and Van Oss approaches, cells of *S. obliquus* exhibited a hydrophilic character, the θ$_w$ value (34.9° ± 0.4) was less than 65° and the ΔG$_{iwi}$ had a positive value (37.23 ± 1.13 mJ m^{-2}) (Table 2). These findings are consistent with previous results reporting the hydrophilic character of various microalgae strains (Ozkan and Berberoglu, 2013). It has been reported that the hydrophobicity of the microbial surface can be attributed to proteins of the cell wall (Vichi et al., 2010). Additionally, the surface of *S. obliquus* appears to behave predominantly as electron donors/Lewis bases with high values of γ$^-$ = 52.57 ± 0.6 mJ m^{-2}. These results indicate also that this strain exhibit a weak electron acceptor character with γ$^+$ = 0.24 ± 0.07 mJ m^{-2}. Previous studies have also demonstrated the electron donor character of several microorganisms, which has been correlated with the presence of phosphate groups in the cell wall (Vichi et al., 2010). These findings are in agreement with the FTIR analyses that confirm the presence of phosphate groups on its cells surface. On the other hand, the θ$_w$ of *S. obliquus* significantly decreased from 34.9° ± 0.4–31.6° ± 0.9 after Pb(II) biosorption (Table 2). This increase can be attributed to the increased density of polar functional groups on the biomass surfaces after the biosorption process (Yalçin et al., 2010). Furthermore, a significant variation was noted in the electron donor and acceptor character after Pb(II)-biosorption (γ$^+$ from 0.24 ± 0.07 to 0.08 ± 0.02 mJ m^{-2}; and γ$^-$ from 52.57 ± 0.6 to 59.79 ± 0.5 mJ m^{-2}) because of the interaction of functional groups in the cells' surface with the Pb(II) ions.

From these results, we can conclude that the biosorption of Pb(II) on the surface of *S. obliquus* implies several chemical and electrostatic interactions, which would occur between the macromolecules that compose the cell surface and the Pb(II) ions (Tran et al., 2017).

3.1.2. Physiological and biochemical response to Pb(II) bioaccumulation

To evaluate the influence of Pb(II) bioaccumulation on the physiological and the biochemical parameters of the used strain for their
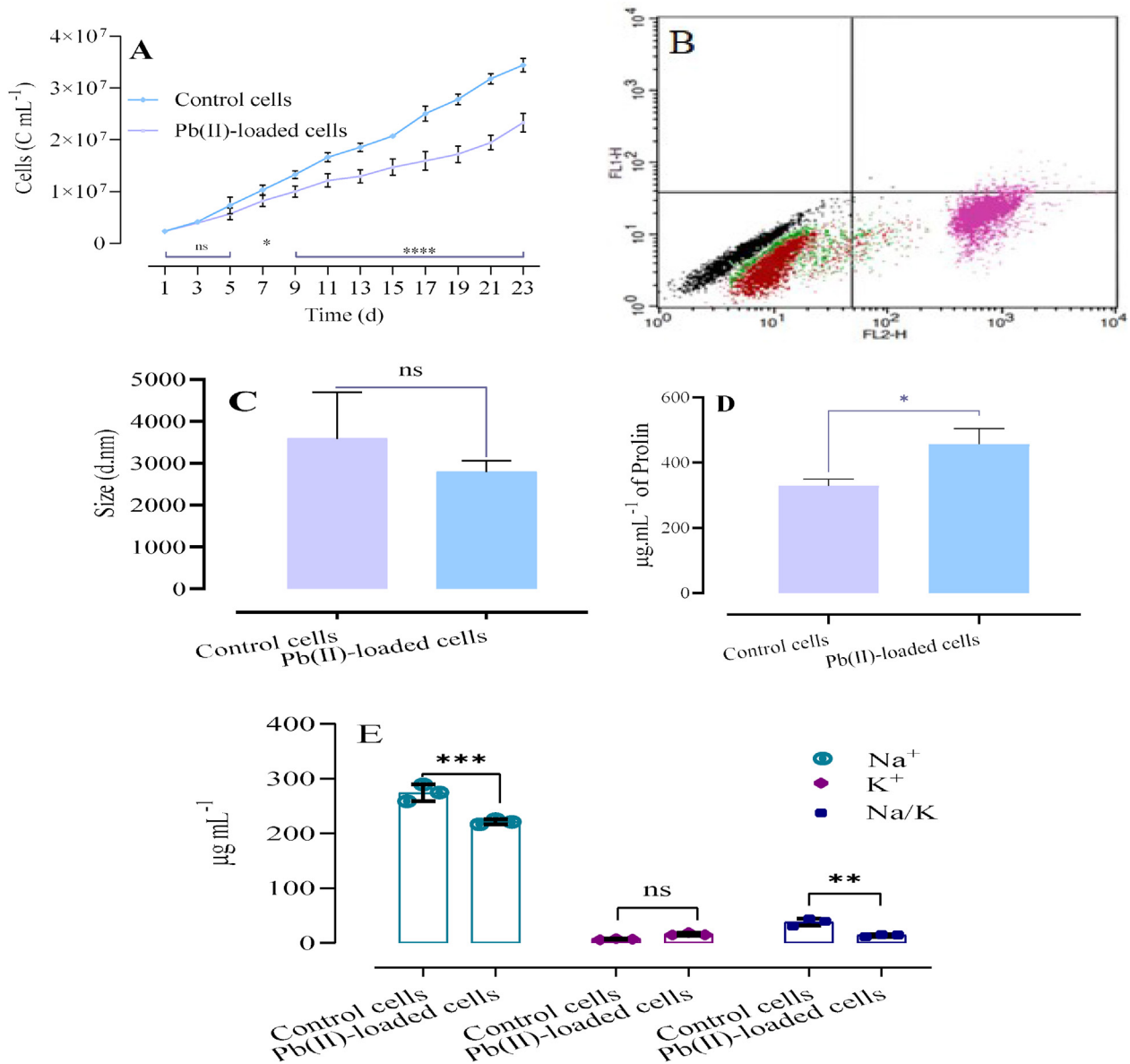
Figure 3. Shows growth kinetics (mean ± S.D, n = 3) (A), (B) illustrate the cytogram of the cells viability: (Black) cells auto-fluorescence canceled (Green) the negative control (96.07%), (Red) after Pb(II)-phycoremediation (90.10 %) and (Pink) heat-inactivated cells. Population moved in the FL_2 channel corresponding to the positive control (0.07 %). UL: Upper Left, UR: Upper Right, LL: Lower Left, LR: Lower Right. (D) displays the Pb(II) effect on the intensity particle size distribution of *S. obliquus* cells. (E) displays the contents of Na^+, K^+ and the ratios of Na/K in control and Pb(II)-loaded cells, the error bar indicates the standard error of the mean (n = 3).

treatment, the growth kinetics, the membrane integrity, and the cell size of *S. obliquus* cultured in control and Pb(II)-doped medium were investigated (Figure 3A). The growth inhibition was monitored throughout the exponential phase to assess the influence of Pb(II) ions on the cell's growth, and not to be confused with growth inhibition related to decreased nutrient availability. During the first week of culture, the growth kinetics of *S. obliquus* in Pb(II)-doped medium showed no significant inhibition compared with control cells. However, from the 7th day of culture, a significant growth inhibition was noticed, and it was maintained at a stationary level from the 13th day of culture. The influence of Pb(II) on the growth of *S. obliquus* was consistent with previous research, such as the study by Li et al. (2021), which reported the inhibitory effect of Pb(II) on the growth of green microalgae.

Table 2. Contact angle values of control (CTR) and Pb(II)-loaded cells (Pb–C), using water (θ_w), formamide (θ_F) and diiodomethane (θ_D), Lifshitz-van der Waals (γ^{LW}), electron-donor (γ^-), electron-acceptor (γ^+) parameters, and surface energies (ΔG_{iwi}).

	Contact angles (°)			Surface tension: components and parameters (mJ m^{-2})			Surface energies
	θ_w	θ_F	θ_D	γ^{LW}	γ^+	γ^-	ΔG_{iwi} (mJ m^{-2})
CTR	34.9 ± 0.4	42.2 ± 0.6	49.5 ± 1.6	34.45 ± 0.9	0.24 ± 0.07	52.57 ± 0.6	37.23 ± 1.13
Pb-c	31.6 ± 0.9*	44.1 ± 0.5^{ns}	36.3 ± 0.6***	41.33 ± 0.3***	0.08 ± 0.02*	59.79 ± 0.5***	44.9 ± 1.2**

*Statistical significance p value <0.05.
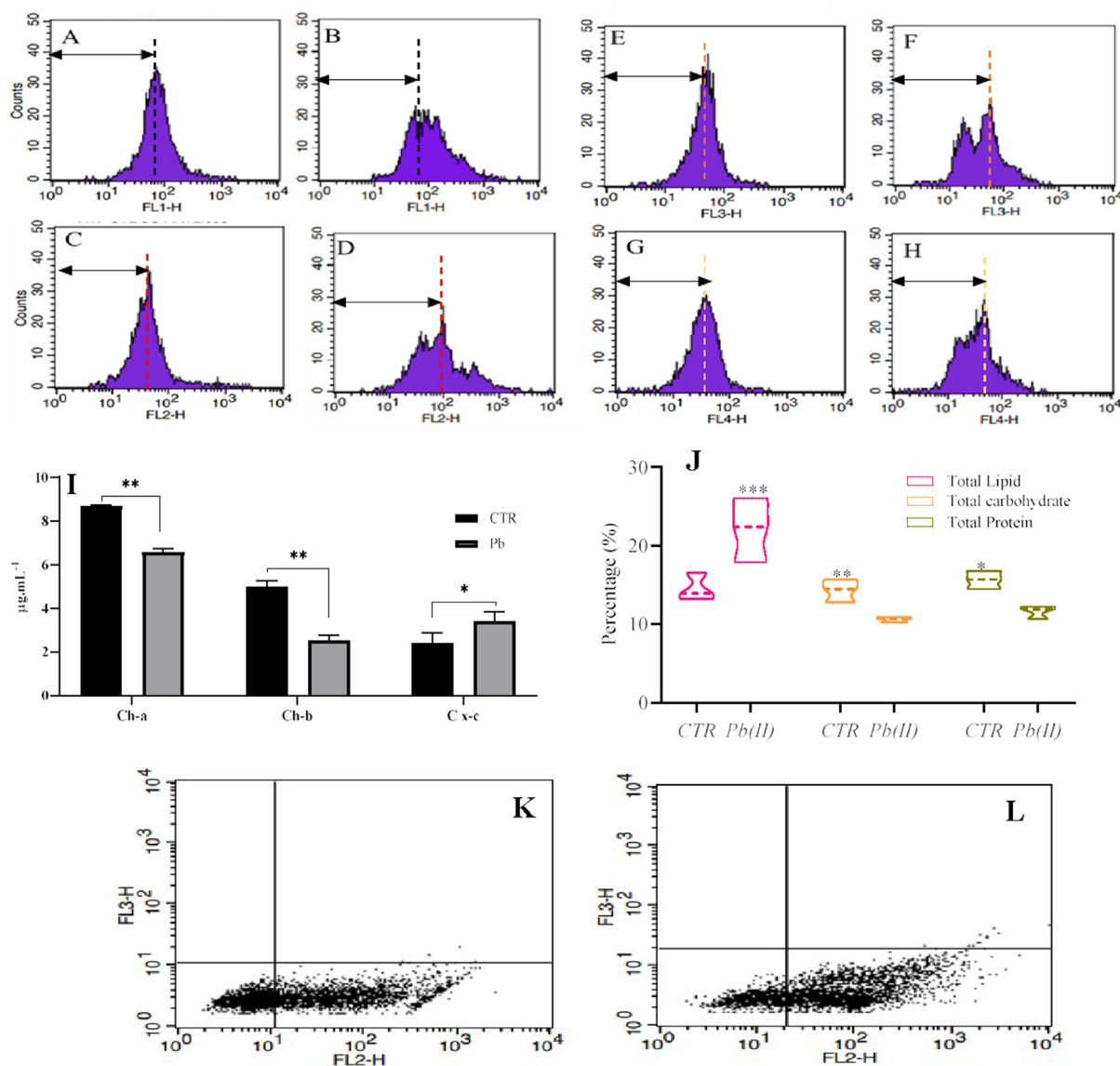
Figure 4. Shows the autofluorescence of native pigments of control cells (A, C, E and G) and (B, D, F and H) and Pb(II)-loaded cells. Figure 4I illustrate the concentration of chlorophyll a (Ch-a), b (Ch-b), and total carotenoids (C x + c) in control (CTR) and Pb(II)-loaded cells. Figure 4 (J) shows the compositions of the total lipid, carbohydrate and protein in control and Pb(II)-loaded cells. Figure 4 (K) and (L) present NR staining dot plots of control and Pb(II)-loaded cells.

At the end of the growth phase, the cell membrane integrity of *S. obliquus* grown in control and Pb(II) doped medium were assessed, and the results are displayed in the cytogram in Figure 3B. The viability of the negative control (cells from the control medium) was at 96.07%. However, the rate of living cells versus the negative control was decreased by 6.3% after exposure to Pb(II) ions. The viability of heat-inactivated cells used as a positive control was 0.07%. Generally, the membrane of living cells excludes the penetration of intercalary agents, while this type of molecule can achieve the intracellular compartment across the cell membrane of dead or damaged cells (Johnson et al., 2013). Therefore, we can conclude that the Pb(II) at the EC$_{50}$ concentration (141 mg L^{-1}) has a low impact on the cell membrane integrity. To our knowledge, there is very little research that has focused the assessment of membrane integrity after Pb(II)-phycoremediation using FCM system. Nazari et al. (2018) reported a significant reduction in viability of *C. vulgaris* treated with reduced graphene-silver oxide nanocomposites. A similar effect was also

observed in *C. vulgaris* exposed to zinc oxide nanoparticles (Suman et al., 2015).

Regarding the osmotic state of *S. obliquus* after Pb(II)-bioaccumulation, the results showed in Figure 3D, revealed that Pb(II) at the EC$_{50}$ concentration induced a non-significative decrease in the diameter and the cells-biovolume. It has been reported by Kim et al. (2016) that a reduction in the biovolume of *Chlorella* cells exposed to a high dosage of magnesium aminoclay (MgAC) compared to the control cells. In contrast, Luis et al. (2006) showed a progressive size increase of *C. reinhardtii* exposed to Cu(II) with a concentration ranging from 0 to 200 μM Romero et al. (2020) reported also that the diameter and the volume of *C. vulgaris* had been enhanced after exposure to silver nanoparticles (AgNPs). The maintenance of cell biovolume of *S. obliquus* used in in the present study can be attributed to various osmoregulatory mechanisms, such as the regulation of ion flows, the accumulation of osmoregulators, or the regulation of the balance between synthesis and

degradation of cellular components (Strange, 2004; Kay, 2017). These three aspects were subsequently verified.

First of all, the Pro content in cells after Pb(II) bioaccumulation showed a considerable increase compared to control cells (Figure 3D), the accumulation of Pro in cells of microalgae under HMs exposure has been documented in some researches. A study by Çelekli et al. (2013) suggested that Cd(II) induces their production in cells of *S. quadricauda*. Similarly, Tripathi et al. (2006) pointed out that the accumulation of Pro in *S. acuminatus* may be an effective strategy to reduce oxidative stress induced by Cu(II) and Zn(II). Likewise, Hamed et al. (2017) showed that both strains *C. sorokiniana* and *S. acuminatus* accumulated Pro under Zn (II) stress. It has been reported that Pro, because of its chemical properties, they can serve as signaling, antioxidants, and osmolytes molecules (Danouche et al., 2022).

Regarding ion flux, the analysis of Na^+, K^+ concentration in *S. obliquus* cells from control and Pb(II)-loaded media (Figure 3E), showed a significant decrease in the concentration of Na^+ ions in Pb(II)-loaded cells compared to control cells. However, no significant change was noted in the concentration of K^+ ions. The finding can be attributed to the flux of ions from the intracellular compartment to the extracellular medium (Diep et al., 2018).

Concerning the regulation between the synthesis and degradation of cellular components, a study of the content of pigments, proteins, lipids, and carbohydrates was also performed. Cells of green microalgae are autofluorescent, their signature can be observed in the red, the orange, and the green channel using FCM system. As shown in Figure 4, Pb(II) ions cause an alteration in the autofluorescence of *S. obliquus*. A shift in autofluorescence of native pigments was observed in the Pb(II)-loaded cells (B, D, F, and H) compared with cells from the control medium (A, C, E, and G). The orange fluorescence is much lower than the chlorophyll autofluorescence, as detected in the red channel. The intensity of orange, green, and red autofluorescence can vary in response to changes in the physiological state of microalgae cells under various oxidative stress conditions (Ying and Dobbs, 2007). According to the above findings, Cheloni and Slaveykova (2013) reported also a change in the autofluorescence of *C. reinhardtii* exposed to copper (Cu(II)), Hg(II), and nanoparticulate Cu(II) oxide.

The spectrophotometric measurements of the pigment content showed that the concentration of Ch-a and Chl-b decreased significantly in cells extract of *S. obliquus* grown in Pb(II)-doped medium compared to cells from the control medium (Figure 4I). The total Chl-a and Chl-b were reduced from 54.08% to 52.5% and from 30.99% to 20.1%, respectively. In contrast, the total carotenoids increased from 14.93% to 27.3% in Pb(II)-loaded cells. In keeping with this finding, Piotrowska-Niczyporuk et al. (2015) reported that the total carotenoids in cells of *Acutodesmus obliquus* was less influenced by Pb(II) as compared to chlorophyll. According to Nazari et al. (2018), the decrease in the chlorophyll content is one of the main indicators of oxidative stress in cells of microalgae. It can be explained by the inhibition of their biosynthesis, by their eventual degradation, or by the alteration of the thylakoid system following the binding of HM to proteins (Carfagna et al., 2013; Piotrowska-Niczyporuk et al., 2015). Regarding the increase of the carotenoids content in Pb(II)-loaded cells, it has been reported that this class of pigments provides protection to photosynthetic membranes against free radicals generated following the HMs bioaccumulation (Piotrowska-Niczyporuk et al., 2015; Rai et al., 2013). Indeed, carotenoids have antioxidant properties, they act as an inhibitor of lipid peroxidation, they increase the stability of the photosynthetic apparatus and protect the integrity of the cell membranes (Pérez-Gálvez et al., 2020).

The biochemical composition of *S. obliquus* biomass from control and Pb(II) doped medium presented in Figure 4J reveals that Pb(II) stimulates the production of lipids, a significant increase in lipids content, which increases from 14.58% in control cells to 22.14% in Pb(II)-loaded cells. Several previous studies support this finding. For example, Nanda et al. (2021) showed an increase in lipid content in *C. sorokiniana* grown under Pb(II) stress. As regards the examination of neutral lipids with the FCM

system. The signal collected in the FL_2 channel is stronger for Pb(II)-loaded cells compared to cells from control medium, meaning an increase in neutral lipids fluorescence in stressed cells of *S. obliquus* (Figure 4K and L). Several microalgae species have been reported to have a strong capacity to accumulate lipid bodies under various stress conditions (Sarkar et al., 2021). Neutral lipids are part of the essential components of membranes such as glycol and phospholipids (Benhima et al., 2018). In this study, the enhancement of natural lipids content in Pb(II)-loaded cells might be an adaptation mechanism against the oxidative stress caused by Pb(II) ions in the intracellular compartment.

Regarding the carbohydrates and proteins content, a significant decrease was noticed in Pb(II)-loaded cells compared to the control. It was from 14.35% to 10.6%. and from 15.68% to 11.6% for the content of carbohydrates and proteins, respectively. These results are consistent with previous research. For example, Napan et al. (2015) reported that lipid yield was higher in *S. obliquus* grown in the presence of different HMs. Similarly, Han et al. (2019) showed that lipid productivity in *S. obliquus* was significantly increased by 27.95%, 19.21%, and 18.63% after supplementation with Fe, Mn, and Mo, respectively. In contrast, Pham et al. (2020) found that Pb(II) concentration around 0.5 and 1 mg L^{-1}, significantly increased the lipids production, yet the increase in Pb(II) concentration to 10 mg L^{-1} showed a reverse effect. Concerning the influence of Pb(II) on the carbohydrates, our findings are in agreement with Belghith et al. (2016) reported also that soluble and insoluble carbohydrates in *D. salina* significantly decrease with increasing Cd(II) concentration. However, Tahira et al. (2019) noticed an increase in total sugar content in *Euglena gracilis* exposed to As(III) ions. Furthermore, the effects of Pb(II) on the proteins content are consistent with the outcomes reported by Piotrowska-Niczyporuk et al. (2015), who noticed a gradual decrease in the contents of soluble and insoluble proteins of *A. obliquus* exposed to Pb(II) ions. Under HMs stress conditions, it was reported a downregulation of genes involved in primary metabolism and proteins synthesis, as well as activation of genes related to autophagy and proteins degradation (Dittami et al., 2009). In the context of biorefineries, the results of the present study are very promising since the selected strain of *S. obliquus* can accumulate natural lipids after Pb(II)-phycoremediation. Therefore, it is possible to use these lipids for the production of third-generation biofuels or their use in other applications.

3.2. Metabolomics response to Pb(II) bioaccumulation

The metabolomic profiling of FAs, saturated hydrocarbons (alkanes), unsaturated hydrocarbons (alkenes), sterols, and other compounds detected in *S. obliquus* cells grown in control, and Pb(II)-doped medium was investigated. Figure 5 summarizes the metabolite profile of control (A) and Pb(II)-loaded cells of *S. obliquus* (B). A total of 54 and 59 putative compounds were detected respectively in the resulting biomasses. In Pb(II)-loaded cells, relative to control cells, a notable increase was observed in the relative abundance of fatty acid methyl esters (FAME) (15%–18%), alkanes (3%–8%), aromatic compounds (2%–13%) and sterols (1%–2%). However, the amount of monounsaturated fatty acids (MUFA) was decreased from 22% in control to 5% in Pb(II)-loaded cells, alkenes were also reduced from 3% to 2%.

In lipidomic studies, the composition and saturation of FAs are among the main characteristics that require examination (Chwastek et al., 2020). As shown in Figure 5C, the composition and the concentration of FAs identified in cells from the control and Pb(II)-doped medium were significantly different. A set of 28 FAs was detected, belonging to 4 sub-classes including SFA (12), MUFA (7), PUFA (1), and FAME (8). It has been reported by Guschina and Harwood (2006) that, within all lipid classes, FAs are the most abundant in cells of microalgae and they are generally the most influenced by HMs stress. As illustrated in Figure 5 C, the most abundant SFAs in control and in Pb(II)-loaded cells were palmitic acid ($C_{16:0}$), pentadecanoic acid ($C_{15:0}$), and stearic acid ($C_{18:0}$). The concentrations of behenic acid ($C_{22:0}$) and melissic acid ($C_{30:0}$) were also equal in both biomasses. However, in control cells, the concentrations of
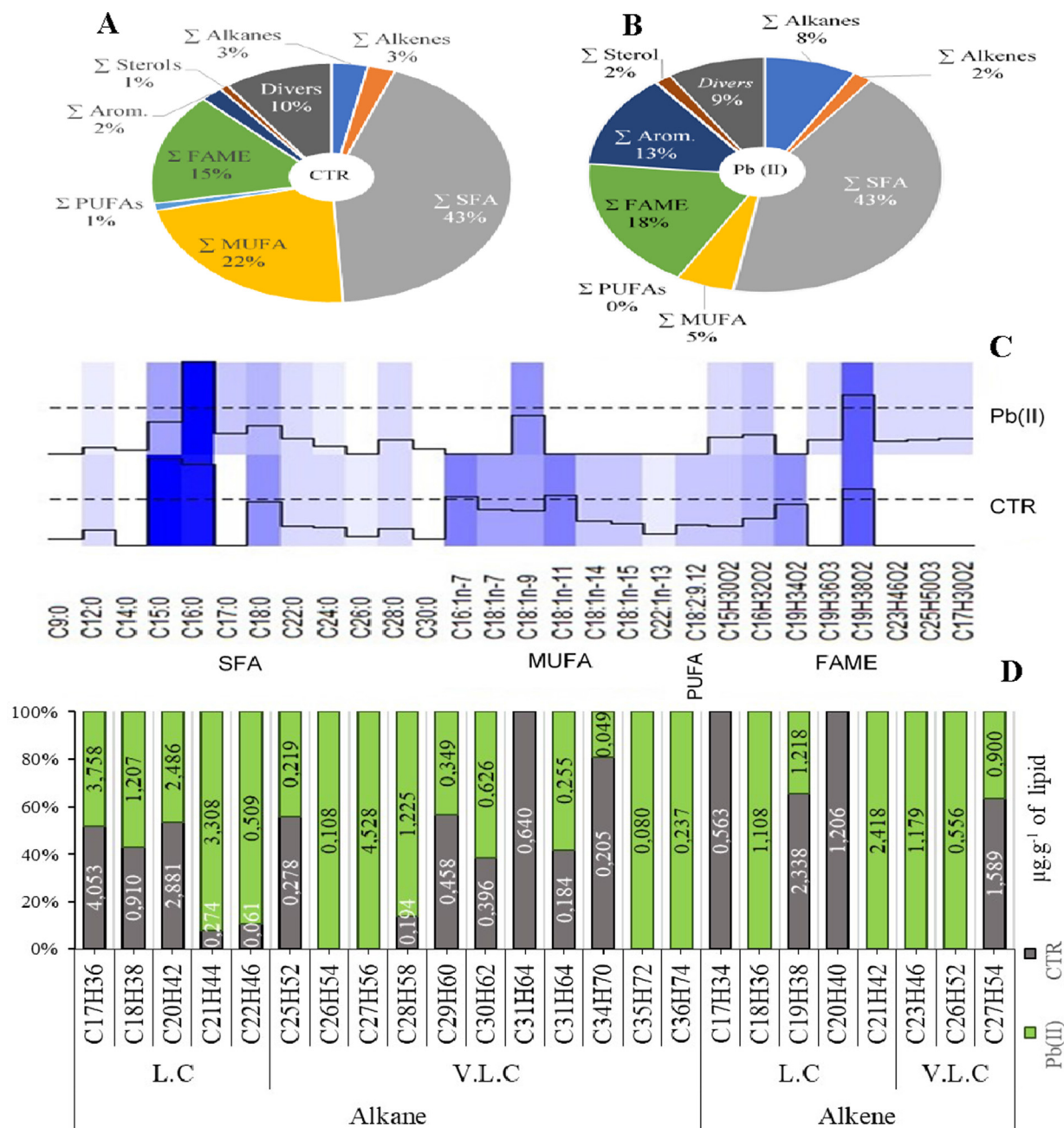
Figure 5. Indicates the level of: Σ alkanes, Σ alkenes, Σ sterols, Fatty acid methyl ester (FAME); monounsaturated fatty acids (MUFA); saturated fatty acids (SFA); Polyunsaturated fatty acids (PUFA); Aromatic compounds (Arom.); divers compounds (Divers)) in control (A) and Pb(II)-loaded (B) cells. (C) shows the distribution of the fatty acid profile (fatty acid methyl ester (FAME); monounsaturated fatty acids (MUFA); saturated fatty acids (SFA); polyunsaturated fatty acids (PUFA)), and (D) illustrates the metabolomic profiling of alkanes and alkenes (very long-chain alkanes (V.L.C); long-chain alkanes (L.C)) in control and Pb(II)-loaded cells.

lauric acid ($C_{12:0}$), pentadecanoic acid ($C_{15:0}$), stearic acid ($C_{18:0}$), lignoceric acid ($C_{24:0}$), and montanic acid ($C_{28:0}$) were higher than in Pb(II)-loaded cells. Pelargonic acid ($C_{9:0}$) and cerotic acid ($C_{26:0}$) were found only in the control cells. The concentration of palmitic acid ($C_{16:0}$) was higher in Pb(II)-loaded cells. As well, the myristic acid ($C_{14:0}$) and margaric acid ($C_{17:0}$) were detected only in the Pb(II)-loaded cells. It has been reported by Atikij et al. (2019) that the myristic acid ($C_{14:0}$) and palmitic acid ($C_{16:0}$) were increased after exposure of *C. reinhardtii* to NaCl stress, suggesting that different promoters had differential effects in the lipid profile. It has been reported also that $C_{14:0}$-mediated N-myristoylation, is among the best characterized types of lipid-mediated protein modifications required for tolerance mechanisms. Indeed, $C_{14:0}$ enrichment in phospholipids mainly phosphatidylcholine can assist the

efficient transmission of external signals to transcriptional machinery, and regulate cellular integrity, ionic and osmotic homeostasis (Jiang et al., 2019). Which, in agreement with the results of the osmotic state of *S. obliquus* after bioaccumulation of Pb(II). Some other previous studies on the biological effects of pollutants on *S. obliquus* have revealed that malic acid was increased. Malate has been found to induce stress tolerance and citrate cycle intermediates, it can also serve as precursors for various biosynthetic pathways, such as gluconeogenesis, lipogenesis, and amino acid synthesis, also as an integral part of the oxidative defense machinery (Du et al., 2017). On the other hand, except for oleic acid ($C_{18:1\omega9}$), all MUFAs were found only in the biomass from the control medium. As regards the PUFA, linoleic acid ($C_{18:2:9,12}$) was detected only in the control biomass. The pathway of FAs biosynthesis leads to the

production of saturated $C_{16:0}$ and $C_{18:0}$, which can further produce various UFAs like oleic acid ($C_{18:1}$), linoleic acid ($C_{18:2}$), and α-linolenic acid ($C_{18:3}$) (Arif et al., 2020). Concerning the FAME, methyl tetradecanoate ($C_{15}H_{30}O_2$), methyl 13-methyltetradecanoate ($C_{16}H_{32}O_2$), and methyl octadecanoate ($C_{19}H_{38}O_2$) were present in both biomasses. Whereas, methyl 20-methyl-heneicosanoate ($C_{23}H_{46}O_2$), methyl 11-(3-pentyl-2-oxiranyl) undecanoate ($C_{19}H_{36}O_3$), methyl 2-hydroxy-tetracosanoate ($C_{25}H_{50}O_3$), and methyl 5,9-hexadecadienoate ($C_{17}H_{30}O_2$) were detected only in Pb(II)-loaded cells. Oppositely, methyl 2-octylcyclopropene-1-heptanoate ($C_{19}H_{34}O_2$) was detected in the control cells.

Few studies have been conducted on the lipidomic profiling of microalgae under HMs exposure. The results of the present study are consistent with previous studies (Rocchetta et al., 2006, 2012; Sibi et al., 2014). For instance, Nanda et al., (2021a) showed that the FAs profiles of *C. sorokiniana* under Pb(II) stress induced an increase in the levels of C_{14}, C_{16}, and $C_{18:1}$, whereas the levels of $C_{16:1}$, C_{18}, $C_{18:2}$, $C_{18:3}$, and C_{20} were reduced compared with control cells. Moreover, ^{1}H-NMR-based lipidomic responses of both *Chlorosarcinopsis bastropiensis* and *Polyedriopsis spinulosa* after bioremediation for Cd(II) and Pb(II) revealed an increase in UFAs (Nanda et al., 2021b). Indeed, FAs can play several physiological functions, like a key bioindicator of the adaptation of the cell membranes to the environmental conditions (Filimonova et al., 2016). It is known that PUFAs are the lipid fraction involved in the maintenance of structural functions. Whereas, SFA and MUFA constitute among others the energy reserves (Olofsson et al., 2012). In fact, the composition of SFAs, MUFAs and PUFAs varies according to species, growth phases and environmental conditions (Breuer et al., 2012). In fact, under HMs exposure, microalgae cells modify their metabolism via an adjustment of the ratio of unsaturated and saturated FAs, in order to reduce the permeability and/or the fluidity of the cell membrane (Lu et al., 2012). Afifudeen et al. (2021) reported that under stressful conditions, partitioning of FAs composition occurs as microalgal cells seek to adapt to the conditions of their surroundings.

Regarding the profile of alkanes and alkenes, a large variation in alkanes and alkenes composition between *S. obliquus* biomass grown in control and Pb(II)-doped media. The relative abundance of alkanes was higher than alkenes. The diversity of the saturated hydrocarbons showed that the content of n-alkanes ranging from n-C_{17} to n-C_{36}, and they are dominated by very-long-chain (V.L.C) alkanes. A total of 15 alkane metabolites were detected in Pb(II)-loaded cells, compared with 11 in control cells. The long-chain (L.C) alkanes are present in both groups, the content of n-C_{17}, n-C_{18}, and n-C_{20} decrease mildly in the Pb(II)-loaded cells. However, a remarkable increase was recorded for n-C_{21} and n-C_{22}. The distribution patterns of V.L.C alkanes varied from 10 in Pb(II)-loaded cells to 6 in control cells. One branched L.C-alkanes (2-Methyl-triacontane ($C_{31}H_{64}$)) was at an equal amount in both biomasses. Four V.L.C alkanes: Hexacosane ($C_{26}H_{54}$), Heptacosane ($C_{27}H_{56}$), Pentatriacontane ($C_{35}H_{72}$), and Hexatriacontane ($C_{36}H_{74}$) were detected only in Pb(II)-loaded cells. Regarding the analysis of the alkene profile, 8 alkenes were detected as follows: in the cells from the control medium, four L.C and one V.L.C alkenes. While, two L.C, and two V.L.C alkenes were detected in Pb(II)-loaded cells. The analysis of alkene data showed that the position of the double bond (C=C) in the alkene from cells grown in the control medium, was located in the first position (1-Heptadecene, 1-Octadecene, 1-Eicosene, 1-Heptacosene), while a change in this position to 9 and 10 (10-Heneicosene ($C_{21}H_{42}$), 9-Tricosene ($C_{23}H_{46}$) and 9-Hexacosene ($C_{26}H_{52}$)) was found in Pb(II)-loaded cells. In the available literature, no previous studies have been investigated the effect of Pb(II) ions on the alkane and alkene profiles of microalgae. It has been reported that hydrocarbons can play several roles in microalgal cells. For example, due to their high hydrophobicity, they contribute to the regulation of the fluidity of photosynthetic membranes and also act in intercellular signaling molecules (Sorigué et al., 2016). It is evident that additional omics research is needed to identify the biochemical pathways responsible for the biosynthesis of alkanes and alkenes by microalgae under HMs stress. Also to identify the mechanisms by which they are involved in managing such oxidative stress.

4. Conclusion

Based on the above considerations, we can deduce that the phycoremediation of Pb(II) using green microalgae strain of *S. obliquus* involves both extracellular biosorption and intracellular bioaccumulation mechanisms. The physicochemical characterization of the control and Pb(II)-loaded cells confirmed the involvement of chemical and electrostatic interactions between the macromolecules constituting the microalgal cell surface and the Pb(II) ions in solution. The comparison of the biochemical and metabolomic profile of *S. obliquus* grown in the control and Pb(II)-doped medium revealed that cells subjected to Pb(II) exposure conditions adjust their metabolism, particularly lipid biosynthesis, in order to reduce the permeability and fluidity of cell membranes. Prevent thereby the intracellular bioaccumulation of Pb(II) ions that may cause various intracellular damages.

References

Afifudeen, C.L.W., Loh, S.H., Aziz, A., Takahashi, K., San Cha, T., 2021. Double-high in palmitic and oleic acids accumulation in a non-model green microalga, *Messastrum gracile* SE-MC4 under nitrate-repletion and -starvation cultivations. Sci. Rep. 11, 1–14.

Akar, T., Anilan, B., Gorgulu, A., Tunali, S., 2009. Assessment of cationic dye biosorption characteristics of untreated and non-conventional biomass: *Pyracantha coccinea* berries. J. Hazard Mater. 168, 1302–1309.

Allen, M.M., 1968. Simple conditions for growth of unicellular blue-green algae on plates. J. Phycol. 4 (1), 1–4.

Ansari, F.A., Gupta, S.K., Bux, F., 2019. Microalgae: a biorefinary approach to the treatment of aquaculture wastewater. In: Application of Microalgae in Wastewater Treatment. Springer, Cham, pp. 69–83.

Arif, M., Bai, Y., Usman, M., et al., 2020. Highest accumulated microalgal lipids (polar and non-polar) for biodiesel production with advanced wastewater treatment: role of lipidomics. Bioresour. Technol. 298, 122299.

Asghari, S., Rajabi, F., Tarrahi, R., Salehi-Lisar, S.Y., Asnaashari, S., Omidi, Y., Movafeghi, A., 2019. Potential of the green microalga *Chlorella vulgaris* to fight against fluorene contamination: evaluation of antioxidant systems and identification of intermediate biodegradation compounds. J. Appl. Phycol.

Ashraf, M.A., Maah, M.J., Yusoff, I., 2014. Soil contamination, risk assessment and remediation. In: Environmental Risk Assessment of Soil Contamination, i (3-56).

Asri, M., El Ghachtouli, N., Elabed, S., Ibnsouda, S., Elabed, A., Silva, B., Tavares, T., 2018. *Wicherhamomyces anomalus* biofilm supported on wood husk for chromium wastewater treatment. J. Hazard Mater. 359 (May), 554–562.

Atikij, T., Syaputri, Y., Iwahashi, H., et al., 2019. Enhanced lipid production and molecular dynamics under salinity stress in green microalga *Chlamydomonas reinhardtii* (137C). Mar. Drugs 17 (8), 484.

Bates, L.S., Waldren, R.P., Teare, I.D., 1973. Rapid determination of free proline for water-stress studies. Plant Soil 39, 205–207.

Belghith, T., Athmouni, K., Bellassoued, K., El Feki, A., Ayadi, H., 2016. Physiological and biochemical response of *Dunaliella salina* to cadmium pollution. J. Appl. Phycol. 28 (2), 991–999.

Benhima, R., El Arroussi, H., Kadmiri, I.M., et al., 2018. Nitrate reductase inhibition induces lipid enhancement of *Dunaliella tertiolecta* for biodiesel production. Sci. World J.

Blaby-Haas, C.E., Merchant, S.S., 2012. The ins and outs of algal metal transport. Biochim. Biophys. Acta 1823 (9), 1531–1552.

Bradford, M.M.B., 1976. Rapid and Sensitive Method for quantitation of microgram quantities of protein utilizing principle of protein-dye binding. Anal. Biochem. 72, 248–254.

Breuer, G., Lamers, P.P., Martens, D.E., Draaisma, R.B., Wijffels, R.H., 2012. The impact of nitrogen starvation on the dynamics of triacylglycerol accumulation in nine microalgae strains. Bioresour. Technol. 124, 217–226.

Carfagna, S., Lanza, N., Salbitani, G., Basile, A., Sorbo, S., Vona, V., 2013. Physiological and morphological responses of lead or cadmium exposed *Chlorella sorokiniana* 211-8K (chlorophyceae). Springer Plus 2 (1), 1–7.

Cervantes-García, D., González-Mendoza, D., Grimaldo-Juárez, O., Aviles-Marin, S., 2011. Changes on proline, phenolics compounds and antioxidants status in *Euglena gracilis* exposed to copper. Afr. J. Microbiol. Res. 5, 5127–5131.

Çelekli, A., Kapi, M., Bozkurt, H., 2013. Effect of cadmium on biomass, pigmentation, malondialdehyde, and proline of *Scenedesmus quadricauda* var. longispina. Bull. Environ. Contam. Toxicol. 91, 571–576.

Chanda, M.J., Benhima, R., Elmernissi, N., et al., 2020. Screening of microalgae liquid extracts for their bio stimulant properties on plant growth, nutrient uptake and metabolite profile of *Solanum lycopersicum* L. Science 10 (1), 1–12.

Cheloni, G., Slaveykova, V.I., 2013. Optimization of the C11-BODIPY581/591 dye for the determination of lipid oxidation in *Chlamydomonas reinhardtii* by flow cytometry. Cytometry 83 (10), 952–961.

Chibueze, C., Chioma, A., Chikere, B., 2016. Bioremediation techniques-classification based on site of application: principles, advantages, limitations and prospects. World J. Microbiol. Biotechnol. 32 (11), 1–18.

Chwastek, G., Surma, M.A., Rizk, S., et al., 2020. Principles of membrane adaptation revealed through environmentally induced bacterial lipidome remodeling. Cell Rep. 32 (12), 108165.

da Silva, T.L., Santos, C.A., Reis, A., 2009. Multi-parameter flow cytometry as a tool to monitor heterotrophic microalgal batch fermentations for oil production towards biodiesel. Biotechnol. Bioproc. Eng. 14 (3), 330–337.

Danouche, M., EL Arroussi, H., El Ghachtouli, N., 2021a. Mycoremediation of synthetic dyes by yeast cells: a sustainable biodegradation approach. Environ. Sustain. 1–18.

Danouche, M., El Ghachtouli, N., El Arroussi, H., 2021b. Phycoremediation mechanisms of heavy metals using living green microalgae: physicochemical and molecular approaches for enhancing selectivity and removal capacity. Heliyon 7, e07609.

Danouche, M., El Ghachtouli, N., El Arroussi, H., 2022. Overview of the management of heavy metals toxicity by microalgae. J. Appl. Phycol.

Danouche, M., El Ghachtouli, N., El Baouchi, A., El Arroussi, H., 2020. Heavy metals phycoremediation using tolerant green microalgae: enzymatic and non-enzymatic antioxidant systems for the management of oxidative stress. J. Environ. Chem. Eng. 8 (5), 104460.

Danouche, M., Ferioun, M., Bahafid, W., El Ghachtouli, N., 2021c. Mycoremediation of azo dyes using *Cyberlindnera fabianii* yeast strain: application of designs of experiments for decolorization optimization. Water Environ. Res. 93 (8), 1402–1416.

Das, D., Chakraborty, S., Bhattacharjee, C., Chowdhury, R., 2016. Biosorption of lead ions (Pb^{2+}) from simulated wastewater using residual biomass of microalgae. Desalination Water Treat. 57 (10), 4576–4586.

Diep, P., Mahadevan, R., Yakunin, A.F., 2018. Heavy metal removal by bioaccumulation using genetically engineered microorganisms. Front. Bioeng. Biotechnol. 6, 157.

Dittami, S.M., Scornet, D., Petit, J.L., et al., 2009. Global expression analysis of the brown alga *Ectocarpus siliculosus* (Phaeophyceae) reveals large-scale reprogramming of the transcriptome in response to abiotic stress. Genome Biol. 10 (6).

Du, C., Zhang, B., He, Y., Hu, C., Ng, Q.X., Zhang, H., Ong, C.N., 2017. Biological effect of aqueous C60 aggregates on *Scenedesmus obliquus* revealed by transcriptomics and non-targeted metabolomics. J. Hazard Mater. 324, 221–229.

Dubois, M., Gilles, K.A., Hamilton, J.K., Rebers, P.A., Smith, F., 1956. Colorimetric method for determination of sugars and related substances. Anal. Chem. 28 (3), 350–356.

El Arroussi, H., Benhima, R., Bennis, I., El Mernissi, N., Wahby, I., 2015. Improvement of the potential of *Dunaliella tertiolecta* as a source of biodiesel by auxin treatment coupled to salt stress. Renew. Energy 77, 15–19.

El Arroussi, H., Benhima, R., El Mernissi, N., Bouhfid, R., Tilsaghani, C., Bennis, I., Wahby, I., 2017. Screening of marine microalgae strains from Moroccan coasts for biodiesel production. Renew. Energy 113, 1515–1522.

Elleuch, J., Hmani, R., Drira, M., Michaud, P., Fendri, I., Abdelkafi, S., 2021. Potential of three local marine microalgae from Tunisian coasts for cadmium, lead and chromium removals. Sci. Total Environ. 799, 149464.

Filimonova, V., Gonçalves, F., Marques, J.C., De Troch, M., Gonçalves, A.M.M., 2016. Fatty acid profiling as bioindicator of chemical stress in marine organisms: a review. Ecol. Indicat. 67, 657–672.

Garrett, R.G., 2000. Natural sources of metals to the environment. Hum. Ecol. Risk Assess. 6 (6), 945–963.

Gupta, V.K., Rastogi, A., 2008. Biosorption of lead from aqueous solutions by green algae Spirogyra species: kinetics and equilibrium studies. J. Hazard Mater. 152 (1), 407–414.

Guschina, I.A., Harwood, J.L., 2006. Lead and copper effects on lipid metabolism in cultured lichen photobionts with different phosphorus status. Phytochemistry 67 (16), 1731–1739.

Hadjoudja, S., Deluchat, V., Baudu, M., 2010. Cell surface characterisation of *Microcystis aeruginosa* and *Chlorella vulgaris*. J. Colloid Interface Sci. 342 (2), 293–299.

Hamed, S.M., Zinta, G., Klöck, G., Asard, H., Selim, S., Abd Elgawad, H., 2017. Zinc-induced differential oxidative stress and antioxidant responses in *Chlorella sorokiniana* and *Scenedesmus acuminatus*. Ecotoxicol. Environ. Saf. 140, 256–263.

Han, S.F., Jin, W., Abomohra, A.E.F., Tu, R., Zhou, X., He, Z., Chen, C., Xie, G.J., 2019. Municipal wastewater enriched with trace metals for enhanced lipid production of the biodiesel-promising microalga *Scenedesmus obliquus*. Bioenergy Res. 12 (4), 1127–1133.

Hassler, C.S., Slaveykova, V.I., Wilkinson, K.J., 2004. Discriminating between intra- and extracellular metals using chemical extractions. Limnol Oceanogr. Methods 2 (7), 237–247.

He, J., Chen, J.P., 2014. A comprehensive review on biosorption of heavy metals by algal biomass: materials, performances, chemistry, and modeling simulation tools. Bioresour. Technol. 160, 67–78.

Huang, L., Bell, R.W., Dell, B., Woodward, J., 2004. Rapid nitric acid digestion of plant material with an open-vessel microwave system. Commun. Soil Sci. Plant Anal. 35 (3-4), 427–440.

Jais, N.M., Mohamed, R.M.S.R., Al-Gheethi, A.A., Hashim, M.K.A., 2017. The dual roles of phycoremediation of wet market wastewater for nutrients and heavy metals removal and microalgae biomass production. Clean Technol. Environ. Policy 19 (1), 37–52.

Jamers, A., Blust, R., De Coen, W., 2009. Omics in algae: paving the way for a systems biological understanding of algal stress phenomena? Aquat. Toxicology 92 (3), 114–121.

Jara, A.D., Martel, A., Molina, C., Nordström, L., Rosa, V.D., Ricardo, D., 2003. Flow cytometric determination of lipid content in a marine dinoflagellate, *Crypthecodinium cohnii*. J. Appl. Phycol. 15, 433–438.

Jena, J., Pradhan, N., Aishvarya, V., et al., 2015. Biological sequestration and retention of cadmium as CdS nanoparticles by the microalga *Scenedesmus*-24. J. Appl. Phycol. 27 (6), 2251–2260.

Jiang, J.Y., Zhu, S., Zhang, Y., Sun, X., Hu, X., Huang, H., Ren, L.J., 2019. Integration of lipidomic and transcriptomic profiles reveals novel genes and regulatory mechanisms of *Schizochytrium* sp. in response to salt stress. Bioresour. Technol. 294, 122231.

Johnson, S., Nguyen, V., Coder, D., 2013. Assessment of cell viability. Curr. Protoc. Cytom. 15 (1), 1–26.

Kay, A.R., 2017. How cells can control their size by pumping ions. Front. Cell Dev. Biol. 5 (May), 1–14.

Kim, B., Praveenkumar, R., Lee, J., Nam, B., Kim, D.M., Lee, K., Lee, Y.C., Oh, Y.K., 2016. Magnesium aminoclay enhances lipid production of mixotrophic *Chlorella* sp. KR-1 while reducing bacterial populations. Bioresour. Technol. 219, 608–613.

Kumar, D., Singh, A., Gaur, J.P., 2008. Mono-component versus binary isotherm models for Cu(II) and Pb(II) sorption from binary metal solution by the green alga *Pithophora oedogonia*. Bioresour. Technol. 99 (17), 8280–8287.

Kumar, K.S., Dahms, H.U., Won, E.J., Lee, J.S., Shin, K.H., 2015. Microalgae - a promising tool for heavy metal remediation. Ecotoxicol. Environ. Saf. 113, 329–352.

Lee, J., Choi, H., Hwang, U., Kang, J., Jai, Y., Il, K., Kim, J., 2019. Toxic effects of lead exposure on bioaccumulation, oxidative stress, neurotoxicity, and immune responses in fish: a review. Environ. Toxicol. Appl. Pharmacol. 68 (March), 101–108.

Leong, Y.K., Chang, J.S., 2020. Bioremediation of heavy metals using microalgae: recent advances and mechanisms. Bioresour. Technol. 303 (December), 122886.

Li, C., Zheng, C., Fu, H., et al., 2021. Contrasting detoxification mechanisms of *Chlamydomonas reinhardtii* under Cd and Pb stress. Chemosphere 274, 129771.

Li, Y., Xia, L., Huang, R., Xia, C., Song, S., 2017. Algal biomass from the stable growth phase as a potential biosorbent for Pb(II) removal from water. RSC Adv. 7 (55), 34600–34608.

Lichtenthaler, H.K., Buschmann, C., 2001. Chlorophylls and carotenoids: measurement and characterization by UV-VIS spectroscopy. Curr. Protoc. Food Anal. Chem. 1 (1), F4.3.1–F4.3.8.

Liu, L., Pohnert, G., Wei, D., 2016. Extracellular metabolites from industrial microalgae and their biotechnological potential. Mar. Drugs 14 (10), 191.

Liyanage, L.M.M., Lakmali, W.G.M., Athukorala, S.N.P., Jayasundera, K.B., 2020. Application of live *Chlorococcum aquaticum* biomass for the removal of Pb(II) from aqueous solutions. J. Appl. Phycol. 32 (6), 4069–4080.

Lu, N., Wei, D., Jiang, X.L., Chen, F., Yang, S.T., 2012. Fatty acids profiling and biomarker identification in snow alga *Chlamydomonas nivalis* by NaCl stress using GC/MS and multivariate statistical analysis. Anal. Lett. 45 (10), 1172–1183.

Luis, P., Behnke, K., Toepel, J., Wilhelm, C., 2006. Parallel analysis of transcript levels and physiological key parameters allows the identification of stress phase gene markers in *Chlamydomonas reinhardtii* under copper excess. Plant Cell Environ. 29, 2043–2054.

Marcilla, A., Gómez-Siurana, A., Gomis, C., Chápuli, E., Catalá, M.C., Valdés, F.J., 2009. Characterization of microalgal species through TGA/FTIR analysis: application to *nannochloropsis* sp. Thermochim. Acta 484 (1-2), 41–47.

Nanda, M., Kumar, K., Kumar, V., 2021a. Micro-pollutant Pb(II) mitigation and lipid induction in oleaginous microalgae *Chlorella sorokiniana* UUIND6. Environ. Technol. Innovat. 23, 101613.

Nanda, M., Jaiswal, K.K., Kumar, V., et al., 2021b. Bio-remediation capacity for Cd(II) and Pb(II) from the aqueous medium by two novel strains of microalgae and their effect on lipidomics and metabolomics. J. Water Proc. Eng. 44, 102404.

Napan, K., Teng, L., Quinn, J.C., Wood, B.D., 2015. Impact of heavy metals from flue gas integration with microalgae production. Algal Res. 8, 83–88.

Nazari, F., Movafeghi, A., Jafarirad, S., Kosari-Nasab, M., Divband, B., 2018. Synthesis of reduced graphene oxide-silver nanocomposites and assessing their toxicity on the green microalga Chlorella vulgaris. BioNanoScience 8 (4), 997–1007.

Olofsson, M., Lamela, T., Nilsson, E., Bergé, J.P., del Pino, V., Uronen, P., Legrand, C., 2012. Seasonal variation of lipids and fatty acids of the microalgae *Nannochloropsis oculata* grown in outdoor large-scale photobioreactors. Energies 5 (5), 1577–1592.

Ong, E.S., Chor, C.F., Zou, L., Ong, C.N., 2009. A multi-analytical approach for metabolomic profiling of zebrafish (*Danio rerio*) livers. Mol. Biosyst. 5, 288–298.

Ozkan, A., Berberoglu, H., 2013. Physico-chemical surface properties of microalgae. Colloids Surf., B 112, 287–293.

Pérez-Gálvez, A., Viera, I., Roca, M., 2020. Carotenoids and chlorophylls as antioxidants. Antioxidants 9, 1–34.

Pérez-Rama, M., Abalde Alonso, J., Herrero López, C., Torres Vaamonde, E., 2002. Cadmium removal by living cells of the marine microalga Tetraselmis suecica. Bioresour. Technol. 84 (3), 265–270.

Pham, T.-L., Dao, T.-S., Bui, H., Pham, T., Ngo, T., Bui, H., 2020. Lipid production combined with removal and bioaccumulation of Pb by *Scenedesmus* sp. green alga. Pol. J. Environ. Stud. 29 (2), 1785–1791.

Piotrowska-Niczyporuk, A., Bajguz, A., Talarek, M., Bralska, M., Zambrzycka, E., 2015. The effect of lead on the growth, content of primary metabolites, and antioxidant response of green alga *Acutodesmus obliquus* (Chlorophyceae). Environ. Sci. Pollut. Res. 22 (23), 19112–19123.

Rai, U.N., Singh, N.K., Upadhyay, A.K., Verma, S., 2013. Chromate tolerance and accumulation in *Chlorella vulgaris* L.: role of antioxidant enzymes and biochemical changes in detoxification of metals. Bioresour. Technol. 136, 604–609.

Randrianarison, G., Ashraf, M.A., 2017. Microalgae: a potential plant for energy production. Geol. Ecol. Landsc. 1 (2), 104–120.

Rocchetta, I., Mazzuca, M., Conforti, V., Balzaretti, V., de Molina, M.D.C.R., 2012. Chromium induced stress conditions in heterotrophic and auxotrophic strains of Euglena gracilis. Ecotoxicol. Environ. Saf. 84, 147–154.

Rocchetta, I., Mazzuca, M., Conforti, V., Ruiz, L., Balzaretti, V., De Molina, M.D.C.R., 2006. Effect of chromium on the fatty acid composition of two strains of Euglena gracilis. Environ. Pollut. 141 (2), 353–358.

Romero, N., Visentini, F.F., Márquez, V.E., Santiago, L.G., Castro, G.R., Gagneten, A.M., 2020. Physiological and morphological responses of green microalgae *Chlorella vulgaris* to silver nanoparticles. Environ. Res. 189 (April).

Saavedra, R., Muñoz, R., Taboada, M.E., Vega, M., Bolado, S., 2018. Comparative uptake study of arsenic, boron, copper, manganese and zinc from water by different green microalgae. Bioresour. Technol. 263 (April), 49–57.

Salama, E.S., Govindwar, S.P., Khandare, R.V., Roh, H.S., Jeon, B.H., Li, X., 2019. Can omics approaches improve microalgal biofuels under abiotic stress? Trends Plant Sci. 24 (7), 611–624.

Samadani, M., Perreault, F., Oukarroum, A., Dewez, D., 2018. Effect of cadmium accumulation on green algae *Chlamydomonas reinhardtii* and acid-tolerant *Chlamydomonas* CPCC 121. Chemosphere 191, 174–182.

Sarkar, R.D., Singh, H.B., Kalita, M.C., 2021. Enhanced lipid accumulation in microalgae through nanoparticle-mediated approach, for biodiesel production: a mini-review. Heliyon 7 (9).

Strange, K., 2004. Cellular volume homeostasis. Adv. Physiol. Educ. 28 (4), 155–159.

Selvi, A., Rajasekar, A., Theerthagiri, J., Ananthaselvam, A., Sathishkumar, K., Madhavan, J., Rahman, P.K.S.M., 2019. Integrated remediation processes toward heavy metal removal/recovery from various environments-A review. Front. Environ. Sci. 7 (May).

Sibi, G., Anuraag, T.S., Bafila, G., 2014. Copper stress on cellular contents and fatty acid profiles in *Chlorella* species. Online J. Biol. Sci. 14 (3), 209–217.

Singh, D.V., Bhat, R.A., Upadhyay, A.K., Singh, R., Singh, D.P., 2021. Microalgae in aquatic environs: a sustainable approach for remediation of heavy metals and emerging contaminants. Environ. Technol. Innovat. 21, 101340.

Sorigué, D., Légeret, B., Cuiné, S., et al., 2016. Microalgae synthesize hydrocarbons from long-chain fatty acids via a light-dependent pathway. Plant Physiol. 171 (4), 2393–2405.

Sudhakar, K., Premalatha, M., 2015. Characterization of micro algal biomass through FTIR/TGA/CHN analysis: application to *Scenedesmus* sp. Energy Source A 37 (21), 2330–2337.

Suman, T.Y., Radhika Rajasree, S.R., Kirubagaran, R., 2015. Evaluation of zinc oxide nanoparticles toxicity on marine algae *Chlorella vulgaris* through flow cytometric, cytotoxicity and oxidative stress analysis. Ecotoxicol. Environ. Saf. 113, 23–30.

Tahira, S., Khan, S., Samrana, S., et al., 2019. Bio-assessment and remediation of arsenic (arsenite As-III) in water by *Euglena gracilis*. J. Appl. Phycol. 31 (1), 423–433.

Tran, N.H., You, S., Hosseini-bandegharaei, A., 2017. Mistakes and inconsistencies regarding adsorption of contaminants from aqueous solutions: a critical review. Water Res. 120, 88–116.

Tripathi, B.N., Mehta, S.K., Amar, A., Gaur, J.P., 2006. Oxidative stress in *Scenedesmus* sp. during short- and long-term exposure to Cu^{2+} and Zn^{2+}. Chemosphere 62, 538–544.

Urrutia, C., Yañez-Mansilla, E., Jeison, D., 2019. Bioremoval of heavy metals from metal mine tailings water using microalgae biomass. Algal Res. 43 (September), 101659.

USEPA, 2016. National primary drinking water regulations. In: EPA 816-F-09-004. U.S.E.P. Agency, United State Environmental Protection Agency. United State. Drinking Water Contaminants, pp. 141–142.

van den Berg, R.A., Hoefsloot, H.C.J., Westerhuis, J.A., et al., 2006. Centering, scaling, and transformations: improving the biological information content of metabolomics data. BMC Genom. 7, 1–15.

Van Oss, C.J., Chaudhury, M.K., Good, R.J., 1988. Interfacial Lifshitz-van der Waals and polar interactions in macroscopic systems. Chem. Rev. 88 (6), 927–941.

Venkata Mohan, S., Ramanaiah, S.V., Rajkumar, B., Sarma, P.N., 2007. Removal of fluoride from aqueous phase by biosorption onto algal biosorbent *Spirogyra* sp.-IO2: sorption mechanism elucidation. J. Hazard Mater. 141 (3), 465–474.

Vichi, S., Gallardo-chacón, J.J., Pradelles, R., Chassagne, D., López-tamames, E., Buxaderas, S., 2010. Surface properties of *Saccharomyces cerevisiae* lees during sparkling wine ageing and their effect on flocculation. Int. J. Food Microbiol. 140 (2-3), 125–130.

Vogler, E.A., 1998. Structure and reactivity of water at biomaterial surfaces. Adv. Colloid Interface Sci. 74, 69–117.

Wang, P., Ng, Q.X., Zhang, H., Zhang, B., Ong, C.N., He, Y., 2018. Metabolite changes behind faster growth and less reproduction of *Daphnia similis* exposed to low-dose silver nanoparticles. Ecotoxicol. Environ. Saf. 163, 266–273.

Wollmann, F., Dietze, S., Ackermann, J.U., Bley, T., Walther, T., Steingroewer, J., Krujatz, F., 2019. Microalgae wastewater treatment: biological and technological approaches. Eng. Life Sci. 19 (12), 860–871.

Wychen, S.V., Laurens, L.M.L., 2017. Total carbohydrate content determination of microalgal biomass by acid hydrolysis followed by spectrophotometry or liquid chromatography. In: Methods in Molecular Biology, pp. 257–284.

Xia, L., Huang, R., Li, Y., Song, S., 2017. The effect of growth phase on the surface properties of three oleaginous microalgae (*Botryococcus* sp. FACGB-762, *Chlorella* sp. XJ-445 and *Desmodesmus bijugatus* XJ-231). PLoS One 12 (10).

Yalçin, E., Çavuşoğlu, K., Kinalioğlu, K., 2010. Biosorption of Cu^{2+} and Zn^{2+} by raw and autoclaved *Rocella phycopsis*. J. Environ. Sci. (China) 22 (3), 367–373.

Yan, X., Liu, M., Zhong, J., Guo, J., Wu, W., 2018. How human activities affect heavy metal contamination of soil and sediment in a long-term reclaimed area of the Liaohe River Delta, North China. Sustainability 10 (2), 1–19.

Ying, Z.T., Dobbs, F.C., 2007. Green autofluorescence in dinoflagellates, diatoms, and other microalgae and its implications for vital staining and morphological studies. Appl. Environ. Microbiol. 73 (7), 2306–2313.

Zehra, T., Priyantha, N., Lim, L.B.L., 2016. Removal of crystal violet dye from aqueous solution using yeast-treated peat as adsorbent: thermodynamics, kinetics, and equilibrium studies. Environ. Earth Sci. 75 (4), 1–15.

Zheng, H., Guo, W., Li, S., et al., 2016. Biosorption of cadmium by a lipid extraction residue of lipid-rich microalgae. RSC Adv. 6 (24), 20051–20057.

Zhou, G.J., Peng, F.Q., Zhang, L.J., Ying, G.G., 2012. Biosorption of zinc and copper from aqueous solutions by two freshwater green microalgae *Chlorella pyrenoidosa* and *Scenedesmus obliquus*. Environ. Sci. Pollut. Res. 19 (7), 2918–2929.